Check for updates

JOURNAL OF SANDWICH STRUCTURES & MATERIALS

Original Article

Analyses of bending performance of innovative paper-based sandwich beams with cup-box core

Journal of Sandwich Structures & Materials
2024, Vol. 26(8) 1684–1706
© The Author(s) 2024

Article reuse guidelines:
sagepub.com/journals-permissions
DOI: 10.1177/10996362241287426
journals.sagepub.com/home/jsm
Sage

Marcus Vinícius Tavares da Costa[1], Mikael Perstorper[1,2] and Johan Vessby[1]

Abstract

Paper-based materials are being alternative candidates to build load-bearing components for the high demanding building sector to be committed to the green transition, but more knowledge of structural mechanics of such components is needed. In this work, three categories of innovative load-bearing sandwich beams with cup-box core fully made of different paper materials were produced, tested and analyzed in four-point bending. The first failure mode was observed at the top facesheets due to the low compressive strength of paper materials; Beams with thin facesheets had premature buckling failure, whereas those with thicker facesheets exhibited ductility reaching higher deflection before the compressive failure. The developed finite element model, calibrated with the experiments for the equivalent bending and shear rigidities, provided figures of the modulus of the facesheet as well as the properties of the core. Furthermore, the compressive plasticity behavior of the facesheets was assessed by fitting the model with load-deflection curves from the tests. Using the model for the structural optimization of the thickness and height of the core, the work suggests optimal values 3 times higher than the original ones.

Keywords

Paper-based materials, sandwich beam, cup-box core, bending test, DIC, finite element modeling

[1]Department of Engineering and Chemical Sciences, Karlstad University, Karlstad, Sweden
[2]Dynalyse AB, Partille, Sweden

Corresponding author:
Marcus Vinícius Tavares da Costa, Department of Engineering and Chemical Sciences, Karlstad University, Karlstad SE-651 88, Sweden.
Email: marcus.tavares@kau.se

Introduction

One of the immediate initiatives globally adopted to tackle the global warming is the implementations of green economy policies,[1] which are linked to the sustainable development goals.[2] The implementations are complex and affects different levels in the society, but the notion has already been started, especially the transition towards the use of renewable products over fossil-based counterparts. Now, an increasing number of products and materials derived from trees are replacing fossil-based alternatives. Typically, around 25% of a harvested tree becomes timber and the remaining large portion becomes pulp-based products, which is the basis for the major contribution of the packaging industries to the development of the pulp and paper sector over the years. These advancements have led to sophisticated manufacturing processes, such as the molded pulp process for the development of molded food packages and similar products.[3] It has been a great step forward because complex geometries made of wood fibers could then be achieved. The processes are versatile and allow to incorporate recycled fibers as well. However, mechanical properties of paper materials are affected by any adjustment in the processes. In the literature, mechanical properties of papers made of different processes have been vastly studied in different aspects.[4] As a brief review, those aspects are, but not limited to, anisotropy properties,[5–7] the process-property relations,[8] asymmetry of strength in tension and compression[9,10] fracture mechanical properties of paper materials,[11,12] moisture dependency for stiffness and strength[13–15] and creep properties of papers.[16–18] Even finite element (FE) models from converting processes to food packages was developed[19] as well as FE simulations to predict the mechanical performance of entire food packages.[20] The knowledge of the mechanics of paper materials is substantial and have now reached a good level of maturity for reliably design food packages from the material level to final products at least for short-lived end-uses.

Other sectors are also exploring the possibility to finetune mechanical properties of paper materials for different long-lived applications. In Sweden, the company WoodTube recently launched a patented hollow stud made of paperboard for partition walls.[21] This initiative opens the door to a new research area to be explored. It also means that the well-stablished knowledge from packaging community should carefully be transferred to the research field of building technology. One challenge in this knowledge transfer is that paperboards are thin materials and structural components are relatively larger than food packages. To make larger structural members out of thin materials, one alternative is through sandwich structures with lightweight cores.[22–24] The cores of such structures can be designed in different shapes - from traditional honeycomb shapes[25] to peculiar cup-box shapes[26] - to adapt different loading conditions.[27] Typically, in building applications, paper-based sandwich structures are commonly made of honeycomb core with hexagonal shape and are primarily evaluated by bending loading cases.[28,29] They are intended to furniture and interior applications, aiming to create lighter furniture to reduce health issues from lifting and moving and saving from furniture transportations costs.[30] For the construction segment, such structures have been used as building envelops and cladding systems.[31] Mechanically, honeycomb cores have higher stiffness perpendicular to the facesheets, greater shear stiffness, and better strength-to-weight ratios compared to other

available core shapes.[32,33] However, their manufacturing processes are not trivial and consist of multiple steps (e.g., expansion processes where thin corrugated sheets are manufactured, glued, stacked, cured, etc.), which may lead to some practical difficulties during assembling of the core. Despite such difficulties, paper honeycomb sandwich structures have demonstrated appealing indicators of mechanical performance per cost offering economic advantages for furniture producers.[34]

Thanks to continuous improvement of molded pulp processes, complex-shaped cores made of paper materials can now be manufactured and studied.[35] It also allows for the production of paper cores in large volumes and more efficiently than expansion processes. In that direction, some other companies in Sweden have developed an innovative sandwich structural element fully made of paper materials for indoor products, such as tables, shelves, doors, and furniture in general.[36] The element, lightweight and stronger, has facesheets of high-strength laminated paperboards made of recyclable and/or virgin wood fibers. The core made of the molded pulp process has a shape like a cup-box (c.f. Figure 1(b)), which can be seen as a variant of the honeycomb core adapted to the new manufacturing process. The main inevitable shape changes include introduction of angles, closing cells and removing sharp corners (round cells) for facilitating the extraction of the core from the mould.

The development of the paper sandwich structural element clearly indicates the increasingly interest for developing structural components made of paper materials for the building sector suitable for mass production, but the mechanical performance of the innovative design of the elements has not been examined by any means. In general, there is obviously a gap in documentation regarding mechanical performance of paper materials in structural-scale products,[31,33] especially those made from mould pulp processes as a nearly developed process compared to other traditional ones. To address this lack of knowledge and evaluate the structural performance of the novel paper sandwich element, the present work aims to study beams from the paper-based sandwich element under bending. This approach not only contributes to filling the existing knowledge gap but also introduces novel paper-based materials in structural engineering applications.

The primary objective of this study is to investigate the bending performance of sandwich beams made of high-strength laminated paperboard facesheets (Smurfit Kappa Sverige AB, Sweden) and Greenwood™ cup-box cores (Ecopals AB and Rottneros Packaging AB, Sweden) under four-point bending conditions. This investigation entailed both an experimental test series coupled with digital image correlation (DIC) and the development of a parametric FE model. The predictions of the model were evaluated against the results obtained from the experimental tests. An important objective of the study was to determine the flexural and shear rigidities of the samples from both experiments and FE modelling. Furthermore, the study included a concise parametric analysis aimed at identifying the optimal geometry of the core of the beam under bending conditions. By combining experimental data and FE simulations, the research provides increased understanding of the bending behavior of these innovative sandwich beams.

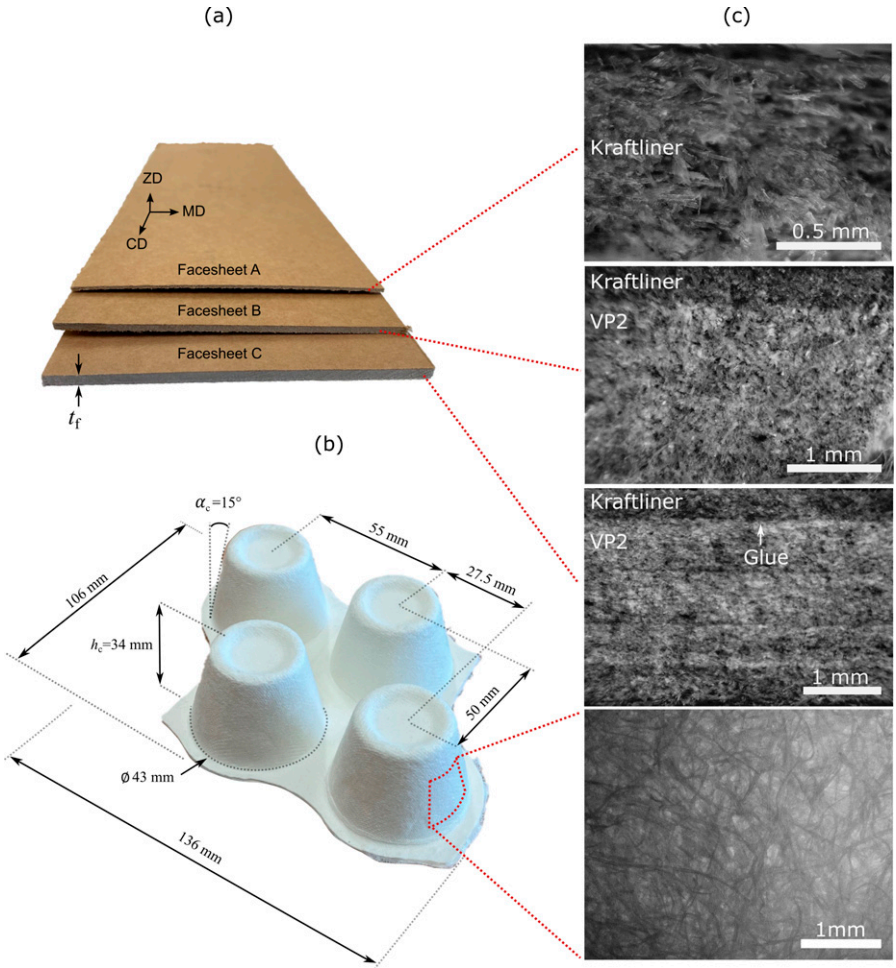

Figure 1. (a) Photographs of the facesheets A, B and C and of (b) a unit of cup-box core showing its shape with dimensions. (c) Micrographs showing the cross section of the facesheets as well as showing in-plane random fiber orientations of the cup-box core.

Materials and methods

Sandwich beams

Facesheet and core materials. The sandwich beams studied were assembled with two facesheets, one at the top and one at the bottom, and one type of core arranged in several units along the beams. The core used was the same for all test specimens while the thickness and orientation of the facesheets varied. The materials for the facesheets, see

Figure 1(a), were provided by the company Smurfit Kappa Sverige AB in three configurations:

(A) Single-ply laminate made from 75% virgin fibers from Northern Sweden and 25% recycled fibers from corrugated board (Kraftliner Brown, Smurfit Kappa, Sweden) with a total thickness t_f = 1.1 mm and the density ρ = 816 kg/m^3,
(B) hybrid three-ply laminate with a total thickness t_f = 2.3 mm and the density ρ = 741 kg/m^3 having two 0.5-mm-ply of Kraftliner Brown at the faces and a 99.5%-recycled-fibers ply in the middle (VP2, Smurfit Kappa, Germany), and
(C) hybrid three-ply laminate with a total thickness t_f = 2.8 mm and the density ρ = 768 kg/m^3 having two 0.5-mm-ply Kraftliner Brown at the faces and a VP2 ply in the middle. This laminate is thicker than B because a water-based glue was added between plies. Then, the laminate was pressed between two rollers in the process. The purpose of the glue is for improving the moisture resistance in a sense of final product application.

The facesheets were manufactured by chemi-thermomechanical pulping (CTMP).[37] In the production process of such facesheets, the material becomes orthotropic with three orthogonal material directions. The machine direction (MD) is the direction parallel to the production line, the perpendicular in plane direction is referred to as the cross direction (CD), and the out of plane direction is the *Z*-direction (ZD). The material coordinate system is exemplified in Figure 1(a) for facesheet A.

The Greenwood core units were manufactured by molded pulp process by Rottneros Packaging AB and contained only virgin fibers. Each unit includes four tapered cups arranged in staggered positions and all connected at the base. Figure 1(b) shows a core unit with its respective dimensions. The unit has a nominal thickness of t_c = 0.8 mm.

Assembly of the sandwich beams. The facesheets were cut with a bench circular saw (Proxxon, Germany) in rectangular dimensions of 802 × 106 mm^2 to accommodate seven cup-box core units in the length direction and one in the width. Figure 2 shows the process of assembling the elements: (a) a solvent-free polyurethane adhesive for wood (Illbruck, Sweden) was applied in the bottom of the core units to be glued to the bottom facesheet,

Figure 2. Process of assembly of the beams: (a) applying adhesive at the bottom of the core units, (b) attaching the core units to the bottom facesheet and applying adhesive on top and (c) pressing the assembly for curing.

(b) the adhesive was then applied at the top of the attached core units. Thereafter the top facesheet was attached and (c) the beams were loaded with 500 N self-load distributed over the top surface for curing during 5 h. In total, eight sandwich beams samples were prepared and categorized in three groups according to their facesheet materials. An important detail for the production of the beams was the orientation of the facesheets. For SE1 and SE3 beams, the facesheets were glued so that the cross direction (CD) was parallel to the length direction of the beam. For the SE2 beams, the machine direction was in parallel to the length direction of the beam. A full specification for each sample is provided in Table 1.

Four-point bending tests

A standard four-point bending test often utilised for investigating stiffness and strength of beams was used to investigate the properties of the eight beams in the study. Before carrying out the bending tests, nine flat-head push pins were glued with a hot-melt adhesive along the top and bottom facesheets at every $d = 67.5$ mm, see Figure 3(a). 3-mm white point markers (GOM, Germany) were attached to the pin heads as references for measuring the beam deflection during loading by means of Digital Image Correlation. Figure 3(b) shows the final beam construction installed in the four-point bending rig. The supports as well as the loading points consisted of steel rollers, each supported at their center with pin connections to allow for rotation and horizontal displacement. The loading points were connected to a spreader beam and further to the load cell via a hinge. Steel plates with dimensions $150 \times 50 \times 5$ mm^3 were inserted between rollers and specimens to reduce stresses and minimize local damage of the face sheets caused by the rollers. The dimensions of the setup are illustrated in Figure 3(c) where the loading span $a = 225$ mm, the total span for bending the beam is $3a = 675$ mm and the total length of the beam is $L = 802$ mm. The span to depth ratio $3a/H$ of approximately 18 was chosen to ensure a reasonable relation between deformation due to pure bending and shear. The tests were performed in a bending testing machine (MEGA 6-3000-200, Form + test Prüfsysteme,

Table 1. Specifications of the sandwich beams.

Beam ID	Sample ID	Facesheet	Height H (mm)	Width W (mm)	Length L (mm)	Mass M (g)	Density[a] (kg/m^3)	‖[b]
SE1	SE1-1	A	36.2	106	802	279	91	CD
	SE1-2	A				288	94	
	SE1-3	A				266	87	
SE2	SE2-1	B	38.7			402	122	MD
	SE2-2	B				390	119	
	SE2-3	B				403	123	
SE3	SE3-1	C	39.8			463	137	CD
	SE3-2	C				467	138	

[a]This is effective densities of the beams calculated as $M/(H \times W \times L)$.
[b]Facesheet orientation along the beams.

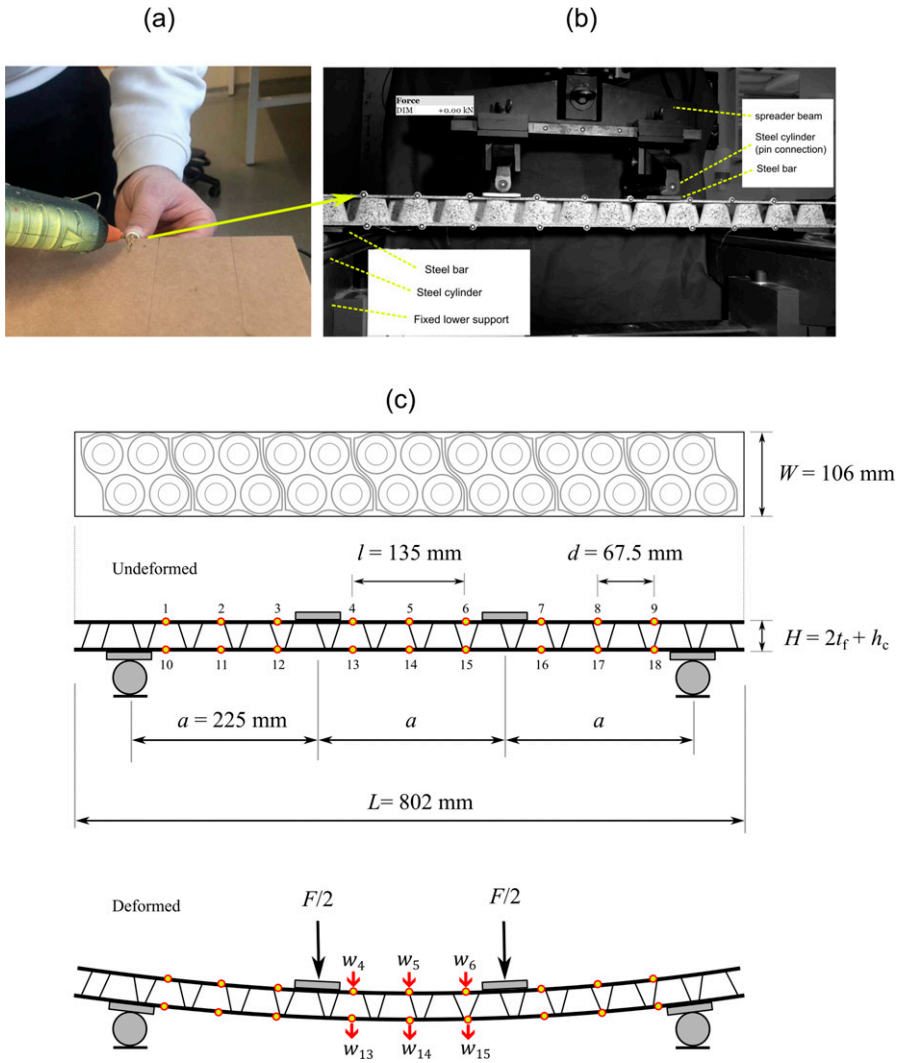

Figure 3. (a) Gluing the push pins in the facesheets, (b) photograph of the four-point bending setup, and (c) illustration of the undeformed and deformed configurations with dimensions.

Germany) with an external 10 kN load cell and displacement control mode with a loading rate of 3 mm/min. During the tests, a stereo-camera system (Aramis 12M, GOM, Germany) was used to measure the displacements at the attached markers by DIC. The system configuration was set as measuring distance of 700 mm, camera angle of 25°, and slider distance of 291 mm. The test climate condition was relative humidity of 38 % and temperature of 20°C.

The equivalent flexural rigidity is calculated from the markers at the mid-span (shear-free) for four-point bending as[38]

$$(EI)_{\text{eq}} = \frac{al^2}{16}\left(\frac{\Delta F}{\Delta w}\right)_{\text{local}} \tag{1}$$

where l is the distance between markers four and six (or 13 and 15) and ΔF is an incremental load within the linear elastic part of the load displacement curve. Δw is the corresponding average local displacement increment from the top and bottom facesheet of the beam respectively so that $w_{\text{loc, top}} = w_5 - \frac{1}{2}(w_4 + w_6)$, $w_{\text{loc, bot}} = w_{14} - \frac{1}{2}(w_{13} + w_{15})$ and $\Delta w = \frac{1}{2}(w_{\text{loc, top}} + w_{\text{loc, bot}})$. The local deflections are illustrated in Figure 3(c).

The equivalent shear rigidity is approximately calculated as

$$(GA)_{\text{eq}} = \frac{a}{2}\left(\frac{\Delta w_{5,14}}{\Delta F} - \frac{23a^3}{48(EI)_{\text{eq}}}\right)^{-1}. \tag{2}$$

Equation (2) is also evaluated at both facesheets. The first term in the parenthesis is the ratio between the mid deflections $\Delta w_{5,14}$ for the force ΔF while the second term includes the length a and the flexural rigidity calculated from equation (1). The expression is derived from the equation for global bending E-modulus (c.f. [38]), which takes into account shear and pure bending deformations.

FE model of the sandwich beams

A flexible finite element model was developed primarily to simulate stiffness and strength of paper-based beams similar to those in the experimental tests, but with different heights, material properties and material thicknesses. A parametric model was developed in the FE software Abaqus. Boundary conditions such as displacements $\boldsymbol{u}$ and rotations $\boldsymbol{\beta}$ are prescribed, see Figure 4(a). For loading, a displacement along the z-axis u_z is prescribed in a top-middle node of a rigid frame while the other translational degrees of freedom are set to 0. The spreader beam is free to rotate around the y-axis β_y and fixed for the rotations in x-axis β_x and z-axis β_z. The interaction between the frame and top steel plates are via coupling of degrees of freedom and are shown in Figure 4(a). For the bottom steel plates, the displacement u_x and the rotation β_y are set free while the remaining degree of freedom is 0. The boundary conditions are defined in this way to resemble the mechanism in the four-point bending experiments. The cup-box core units and the facesheets are assumed to fully interact which is ensured by means of a tie constraint. Between the plates and the facesheets, a penalty contact formulation is defined with the coefficient of friction set to 0.3. The steel plates are modelled by means of rigid elements and the facesheets and core units as continuum shell elements with eight nodes (denoted SC8). A finite strain formulation is used to simulate any local large deformation. In particular, the local failures mainly observed at the top facesheets shown later in Figure 8(b). Figure 4(b) illustrates the meshing for all components. A mesh convergency analysis was performed showing that the relative error is approximately 1% for the mesh in Figure 4(b).

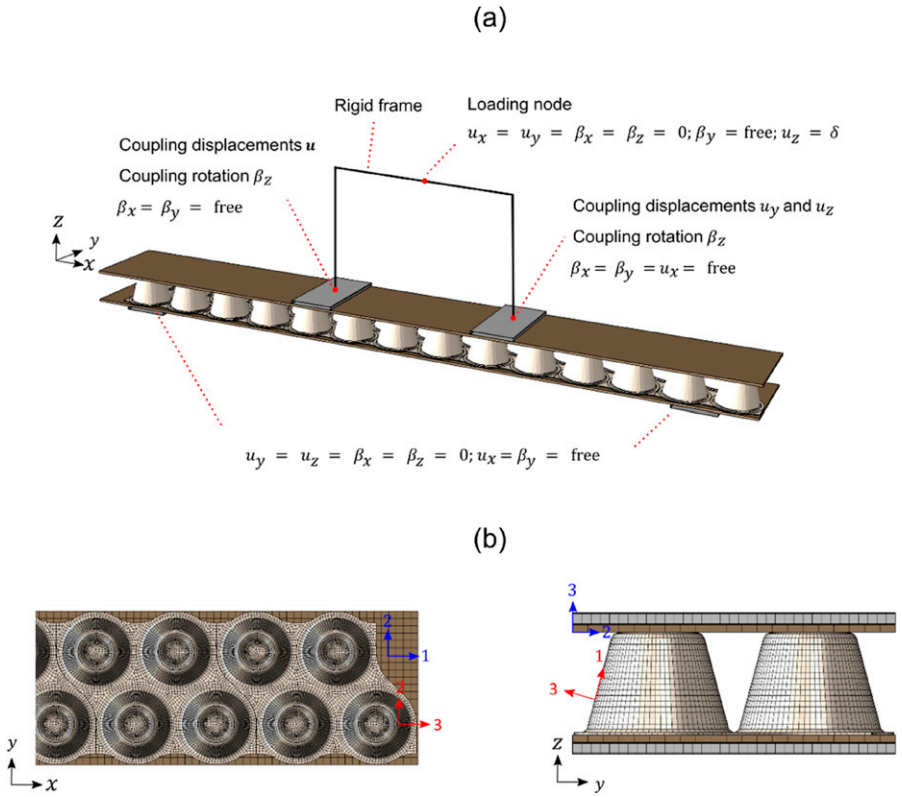

Figure 4. FE model: (a) geometry, boundary conditions and (b) meshing. The 1-2-3 coordinate systems indicate the material orientation for the facesheets (blue) and the core (red).

The 1-2-3 coordinate systems in Figure 4(b) indicate the local material orientations. The core is modelled assuming in-plane isotropic linear elastic material, so called transverse isotropic material. During bending, the facesheets at the bottom are subjected to tension while the facesheets at the top are compressed. As paper-based materials typically have lower strength in compression compared to tension,for example,[10] this must be considered to be able to capture the first failure mode in the FE simulations.

The facesheets in the bottom are modelled with a linear orthotropic material and the ones in the top are assumed to possess orthotropic elastoplastic material properties. The total strain, ε, in the top sheet is obtained as

$$\boldsymbol{\varepsilon} = \boldsymbol{\varepsilon}^{\mathrm{e}} + \boldsymbol{\varepsilon}^{\mathrm{p}} \text{ in } \Omega_{\text{top facesheets}} \tag{3}$$

where $\boldsymbol{\varepsilon}^{\mathrm{e}}$ are the elastic strains and $\boldsymbol{\varepsilon}^{\mathrm{p}}$ the plastic strains. The yield criterion is defined as

$$f(\boldsymbol{\sigma}, \boldsymbol{\varepsilon}^{\mathrm{p}}) = \sigma_{\mathrm{eq}}(\boldsymbol{\sigma}) - \sigma_{\mathrm{Y}}(\boldsymbol{\varepsilon}^{\mathrm{p}}) \leq 0 \tag{4}$$

where Hill's equivalent stress is[39,40]

$$\sigma_{\mathrm{eq}}(\boldsymbol{\sigma}) = \left[F(\sigma_{\mathrm{CD}} - \sigma_{\mathrm{ZD}})^2 + G(\sigma_{\mathrm{ZD}} - \sigma_{\mathrm{MD}})^2 + H(\sigma_{\mathrm{MD}} - \sigma_{\mathrm{ZD}})^2 + 2L{\sigma_{\mathrm{CDZD}}}^2 + 2M{\sigma_{\mathrm{ZDMD}}}^2 + 2N{\sigma_{\mathrm{MDCD}}}^2\right]^{1/2} \tag{5}$$

with Hill's coefficients as

$$F = \frac{1}{2}\left(\frac{1}{R_{\mathrm{CD}}^2} + \frac{1}{R_{\mathrm{ZD}}^2} - \frac{1}{R_{\mathrm{MD}}^2}\right)$$

$$G = \frac{1}{2}\left(\frac{1}{R_{\mathrm{ZD}}^2} + \frac{1}{R_{\mathrm{MD}}^2} - \frac{1}{R_{\mathrm{CD}}^2}\right)$$

$$H = \frac{1}{2}\left(\frac{1}{R_{\mathrm{MD}}^2} + \frac{1}{R_{\mathrm{CD}}^2} - \frac{1}{R_{\mathrm{ZD}}^2}\right)$$

$$L = \frac{3}{2R_{\mathrm{CDZD}}^2}$$

$$M = \frac{3}{2R_{\mathrm{MDZD}}^2}$$

$$N = \frac{3}{2R_{\mathrm{MDCD}}^2} \tag{6}$$

where the R's are the anisotropic yield stress ratios for the material directions. Here, R values for their respective material directions were estimated by literature values of normal and shear yield stresses[13,41] and are tabulated in Table 2. The hardening function $\sigma_{\mathrm{Y}}(\boldsymbol{\varepsilon}^{\mathrm{p}})$, calibrated from the bending tests, is defined as nonlinear following the procedure given in[14]

$$\sigma_{\mathrm{Y}}(\boldsymbol{\varepsilon}^{\mathrm{p}}) = \sigma_{\mathrm{Y0}} + K\left(1 - \exp\left[-n\varepsilon_{\mathrm{eq}}^{\mathrm{p}}\right]\right) \tag{7}$$

where the initial yield stress is σ_{Y0} and the equivalent plastic strain (PEEQ) is

$$\dot{\varepsilon}_{\mathrm{eq}}^{\mathrm{p}} = \sqrt{\frac{2}{3}\,\dot{\boldsymbol{\varepsilon}}^{\mathrm{p}} : \dot{\boldsymbol{\varepsilon}}^{\mathrm{p}}} \tag{8}$$

where $\dot{\boldsymbol{\varepsilon}}^{\mathrm{p}} = [\dot{\varepsilon}_{\mathrm{MD}}^{\mathrm{p}}, \dot{\varepsilon}_{\mathrm{CD}}^{\mathrm{p}}, \dot{\varepsilon}_{\mathrm{ZD}}^{\mathrm{p}}, \dot{\varepsilon}_{\mathrm{MDZD}}^{\mathrm{p}}, \dot{\varepsilon}_{\mathrm{CDZD}}^{\mathrm{p}}, \dot{\varepsilon}_{\mathrm{MDCD}}^{\mathrm{p}}]^{\mathrm{T}}$. The coefficient K and exponent n are fitting parameters. The flow rule is then calculated as

$$\dot{\boldsymbol{\varepsilon}}^{\mathrm{p}} = \dot{\lambda}\frac{\partial f}{\partial \boldsymbol{\sigma}} \tag{9}$$

where $\dot{\lambda}$ is the rate of the plastic multiplier. To fit the FE model to the experimental tests, some material properties were directly extracted from the bending tests. For example, the

Table 2. Non-calibrated elastic constants and R values estimated from the literature[4,13,35,41] for the FE modeling.

Facesheet					Core			
E_{ZD} (MPa)	ν_{MDCD} (-)	ν_{MDZD} (-)	ν_{CDZD} (-)	$G_{MDZD,CDZD}$ (MPa)	E_3 (MPa)	ν_{12} (-)	$\nu_{13,23}$ (-)	$G_{13,23}$ (MPa)
50	0.15	0.01	0.02	120	30	0.17	0.01	150
R_{MD} (-)	R_{CD} (-)	R_{ZD} (-)	R_{MDCD} (-)	$R_{MDZD,CDZD}$ (-)				
1.5	1	0.03	0.6	0.17				

elastic modulus of the facesheets E_1 was calibrated using equation (1) by fitting the local bending stiffness $\left(\frac{\Delta F}{\Delta w}\right)_{\text{local}}$ obtained from the FE model to those from the experiments. In order to do this in an efficient way, the FE model contains reference nodes which are located at the same positions as the DIC markers. Also, the facesheet E_2 was calculated based on the assumption that the E-modulus in the MD-direction is two times the E-modulus in the CD-direction.[4] The in-plane elastic moduli of the core $E_{1,2}$ (a notation that stands for a contraction of "E_1 and E_2") and the in-plane shear modulus $G_{12} = E_{1,2}/2(1 + \nu_{12})$ were calibrated by fitting $(GA)_{\text{eq}}$, so that the global displacements from the model fitted those from the experimental tests. Properties with limited influence on the elastic response for the presented bending setup were estimated based on literature references and are also tabulated in Table 2. The elastic moduli E, Poisson ratios ν and shear moduli G were based on litterature for facesheets[4] and core[35]; the subscripts refer to the manufacturing material directions for the facesheets and the 1-2-3 coordinate systems (in red in Figure 4(b)) for the core.

Results and discussion

FE model calibration

The equivalent flexural and shear rigidities calculated from the experimentally obtained results are tabulated in Table 3 and visualized in Figure 5(a). The high flexural rigidity $(EI)_{\text{eq}}^{\text{exp}}$ in the SE2 beams is due to the fact that the facesheet in that group have MD orientation along the beam, while the others have CD orientation along the beam. For the E-modulus of facesheet in the beam direction, the FE model was calibrated by matching $\left(\frac{\Delta F}{\Delta w}\right)_{\text{local}}$ in equation (1) with the mean of the experimentally obtained results for each beam configuration. The calibrated FE model results in elastic moduli of the facesheets were

Table 3. Experimental results and calibrated material properties for FE-model.

	Facesheet				Core			
Sample ID	$(EI)_{\text{eq}}^{\text{exp}}$ (Nm^2)	E_1^{an} (GPa)	E_1^{FE} (MPa)	E_2^{FE} (MPa)	$(GA)_{\text{eq}}^{\text{exp}}$ (kN)	$(GA)_{\text{eq}}^{\text{FE}}$ (kN)	$E_{1,2}^{\text{FE}}$ (MPa)	G_{12}^{FE} (MPa)
SE1-1	269	3700			10.8			
SE1-2	258	3550			(17.7)			
SE1-3	249	3430			11.0			
SE1-avg	259	3560	3300	6600	10.9	10.9	1740	756
SE2-1	756	4590			19.4			
SE2-2	741	4500			22.3			
SE2-3	749	4550			21.7			
SE2-avg	748	4550	4200	2100	21.1	21.1	1640	702
SE3-1	474	2310			19.3			
SE3-2	533	2600			27.2			
SE3-avg	503	2460	2350	4700	23.2	23.2	1660	711

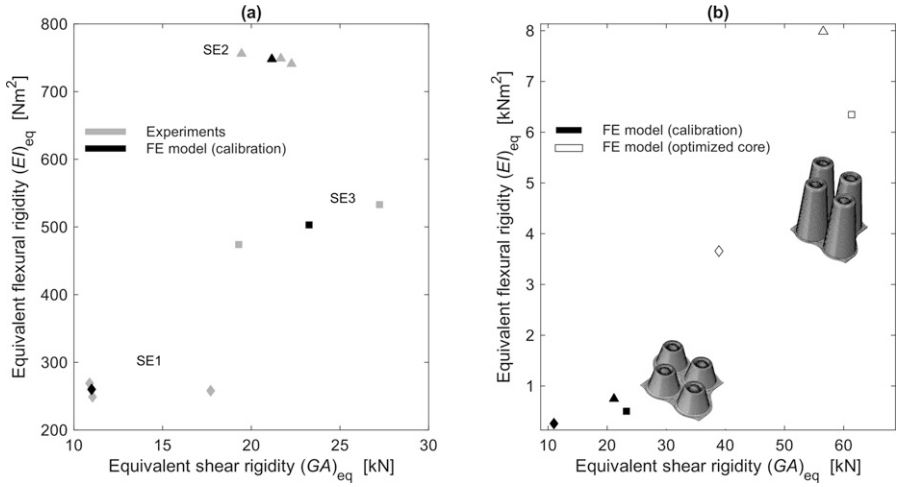

Figure 5. Experiments and FE results of flexural and shear rigidities for SE1 (diamonds), SE2 (triangles) and SE3 (squares): (a) calibrated values from FE models over rigidities of all experiments and (b) the calibrated rigidities values over the rigidities with optimal core geometry from the optimization studies.

$E_1^{\mathrm{FE}} = 3300$, 4200 and 2350 MPa for SE1, SE2 and SE3, respectively. From the experimental tests, values of elastic moduli of the facesheets E_1^{an} were calculated analytically by dividing the result from equation (1) over the second moment of inertia obtained as $I \approx 2\left[\frac{Wt_{\mathrm{f}}^3}{12} + (Wt_{\mathrm{f}}) \cdot \left(\frac{H}{2} - \frac{t_{\mathrm{f}}}{2}\right)^2\right]$, which leads to $E_1^{\mathrm{an}} = 3560$, 4550 and 2460 MPa for SE1, SE2 and SE3, respectively. By comparing the two it can be concluded that the analytical results are 8, 8 and 4% higher than the modulus of elasticity obtained from the FE simulations. Overall, the main reason for the difference is that the simplified analytical evaluation disregards any contribution from the core to the overall bending stiffness of the beam. The variation in bending stiffness for each beam configuration was higher (CV = 4%–8%), than what is typical for the E-modulus of paperboard (CV = 1%–2%). Other explanations are variation in the assembly of the beams, position of markers and loading set-up. The evaluated shear rigidity $(GA)_{\mathrm{eq}}^{\mathrm{exp}}$ has a considerable variation in each configuration with a CV ranging from 6% to 17%. It can also be noted that the shear rigidity was higher for the beams with thicker face sheets. This indicates that the shear rigidity of the beam does not only come from the core. The most important material parameter to influence the shear rigidity of the core unit is the in-plane elastic moduli of the core $E_{1,2}$. The calibrated in-plane elastic moduli of the core were $E_{1,2}$ = 1740, 1640 and 1660 MPa for SE1, SE2 and SE3, respectively. One sample (SE1-2) was neglected in the calibration for the SE1 group as it shown much higher value of $(GA)_{\mathrm{eq}}$ than the other two, see Table 2, and thus it was considered as an outlier. On top of difficulties in precisely positioning of markers on the beams for deformation measurement, SE1 beams had very thin facesheet thickness $t_{\mathrm{f}} \approx 1$ mm and it led to some geometric instability issues during the tests, such as

twisting of the sandwich beams due to property asymmetry, non-centered samples and/or local deformation at supports.

The main purpose for cores in bending is their shear properties. By averaging out the equivalent shear rigidity of cup-box core in Tables 2, it becomes $(GA)_{eq} \approx 18.5$ kN for a core density of $\rho_c = 35$ kg/m^3, which is higher than figures of Polyisocyanurate core foam ($\rho_c = 32$ kg/m^3) with $(GA)_{eq} \approx 7.5$ kN having similar density.[42] For paper honeycomb cores, the comparison is more sensitive because of experimental conditions (e.g., relative humidity) and core densities that may vary from studies to studies. However, as an attempt, the cup-box core performed worse than kraft paper honeycomb with $(GA)_{eq} \approx$ 36-119 kN[32] and $\rho_c = 23$ kg/m^3 and way better than Testliner paper honeycomb $(GA)_{eq} \approx 0.03$ kN.[33] It is worth mentioning that the paper thickness of the latter is only 0.23 mm, which may limit their mechanical performance.

Load-displacement relations

Figure 6 shows the force-deflection curves at mid-span at the bottom and top facesheets for both experiments and simulations. As shown in the experiments, SE1 beams had a short plasticity range before the sudden drop in force level, while SE2 and SE3 developed significant plastic deflection before the drop in force, indicating a more ductile behavior. The failure in SE1 was caused by local buckling of the thin compressed top facesheets for all three tested specimens. The buckling was observed in the constant moment region in the vicinity of one of the two loading points. The failure was initiate due to compression yielding in intermittent regions of the facesheets without support of the core and, subsequently, buckling behavior occurred due to the thin thickness of the facesheets. The buckling behaviour was diagonal following the staggered pattern of the cups in the core, see Figure 8.

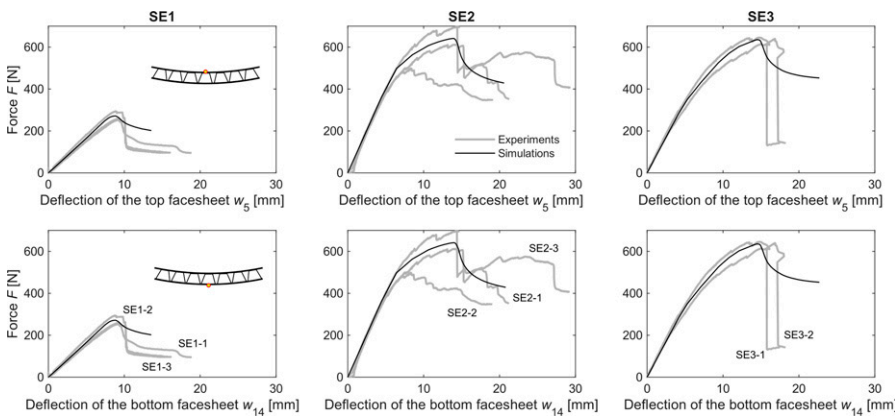

Figure 6. Force-deflection diagrams for all eight test samples along with results from FE simulations of each beam configuration.

The sample SE2-2 exhibited low strength caused by delamination of a section of the facesheet material, as shown in Figure 8(a). Similarly, SE3-1 experienced delamination failure, but it occurred after the compressive failure of the top facesheet, which did not significantly affect its strength. In the non-linear displacement range of samples SE2-1, SE2-3, SE3-1 and SE3-2, small kinks in force graphs can be observed. These kinks are caused by stress redistribution in turn emanating from effects of localized high stress levels near the edges of the cups and minor slippage at the supports. The stress concentrations in the core are plotted as von Mises stress in Figure 8(e) for a beam of the type SE2 at peak force. Although the post peak behavior varies among the samples, a sudden drop in force after reaching the peak force is common in all cases, primarily due to the compression failure in the top facesheet. Results from FE simulations (solid black lines) showed good agreement with the experimental force-deflection graphs in several aspects: (i) they accurately captured the initial linear elastic behavior, which was expected as this region was used for calibrating the model, (ii) they effectively simulated the development of the plastic regions, and (iii) they successfully predicted the beams peak load. It is important to note that the small kinks observed in the experimental curves are not reflected in the FE-simulations. This is because phenomena like minor cracks in the glue line, small delamination within the material and support slip were not accounted for in the FE model. However, the stress concentrations observed in the FE-model within the core do indicate critical zones that could lead to local damages.

In Figure 7, the displacements from all DIC markers w along with the FE predictions are illustrated at a specific load level within the linear elastic region and the peak force of the load-displacement curves for each beam configuration. Two main observations are (i) the slightly changing curvature in the vicinity of the support plates at the displacements in the linear region and (ii) the local failure of the compressed facesheet at peak force. The first is caused by the shear stiffness provided by the core units while the latter indicates that better properties in the top facesheet could increase the load bearing capacity.

In Figure 8(c) the equivalent plastic strain in the top facesheets is presented at the peak force and post-peak force, set to 80% of the peak force, for the beam configurations. SE1 shows a higher and localized PEEQ already at the peak force compared to the others having more uniformly distributed PEEQ. It explains the premature failure of SE1 seen in the experiments. At post-peak force, the buckling failure develops diagonally and close to the top steel plates as seen in the experiments; The main failures in the top facesheets are illustrated in Figure 8(b).

Compressive stress-strain curves of the facesheets from simulations

For the plasticity region in the model, the main inputs are values of yield stresses and plastic strains of the top facesheets. The tabulated set of values in Abaqus that provided good fit to the experimentally obtained results presented in Figures 6 and 7 are plotted as markers in Figure 9. The values were calibrated until the buckling appearance and therefore the compressive yield strengths at buckling onset are the last data points in graph. As an example, Figure 8(d) shows the compressive stress in the top facesheet in

SE2 at peak force. The values ($\sigma_x \approx -10$ MPa) in the middle section are similar to the last data point in Figure 9.

The facesheet A has only one value for initial yield stress σ_{Y0} because it experienced buckling at loads lower than those causing plasticity to develop in the top facesheet. On the contrary, facesheets B and C have some data in the plastic region. The shapes of the hardening functions fitted in Figure 6 by using equation (7) are $K = 4$ MPa and $n = 190$ for facesheet B and $K = 3$ MPa and $n = 400$ for facesheet C.

By comparing the materials, the initial yield stress in the CD-direction of the facesheet A drops by a factor of 3.5 to the hybrid paper material facesheet C. In the same direction, the figures can be compared with the literature, but in tension behaviour. Li et al.[10] found that the stress-strain curves in tension and compression of laminated paperboards do not differ much between the MD and the CD-direction, which permits making comparisons of our compression strain-strain curves to tensile stress-strain curves as tensile tests have more data in the literature. For example, Malin et al.[13,14] have studied tested similar paperboards. Analyzing the facesheet A as it has a conventional composition with only virgin wood fibers, the initial yield stress has similar values as Scandinavian duplex FBB multiply boards, which indicates that the alternative way of using the FE model of the sandwich beam to estimate the material properties are reliable. The CD-modulus of facesheet A $E_1^{FE} = 3250$ MPa is also in the range as many types of paperboards listed in Table 2.1 in.[4]

Structural optimization of the core material

In this section, the model is exploited to optimize the geometry of the core in the beams subjected for the four-point bending test. This is done by maximizing the initial global

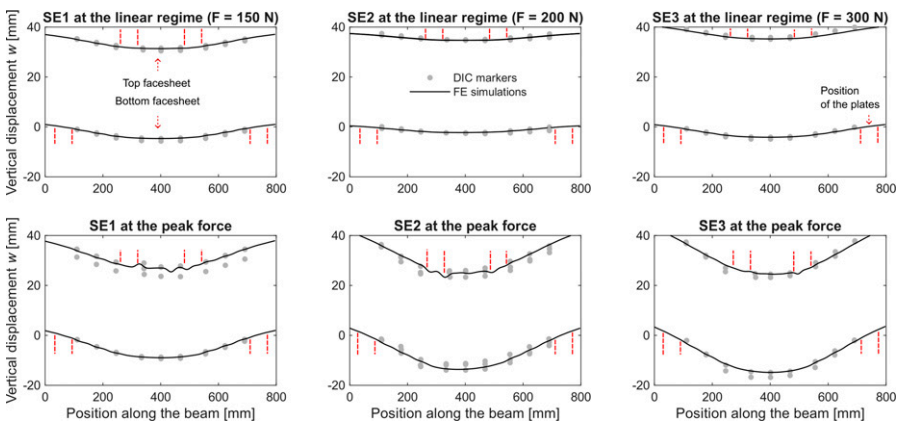

Figure 7. Vertical displacements of the facesheets along the beams at the linear regime and the peak force. The light grey dots are from DIC target measurements and the black solid curves are from the simulations.

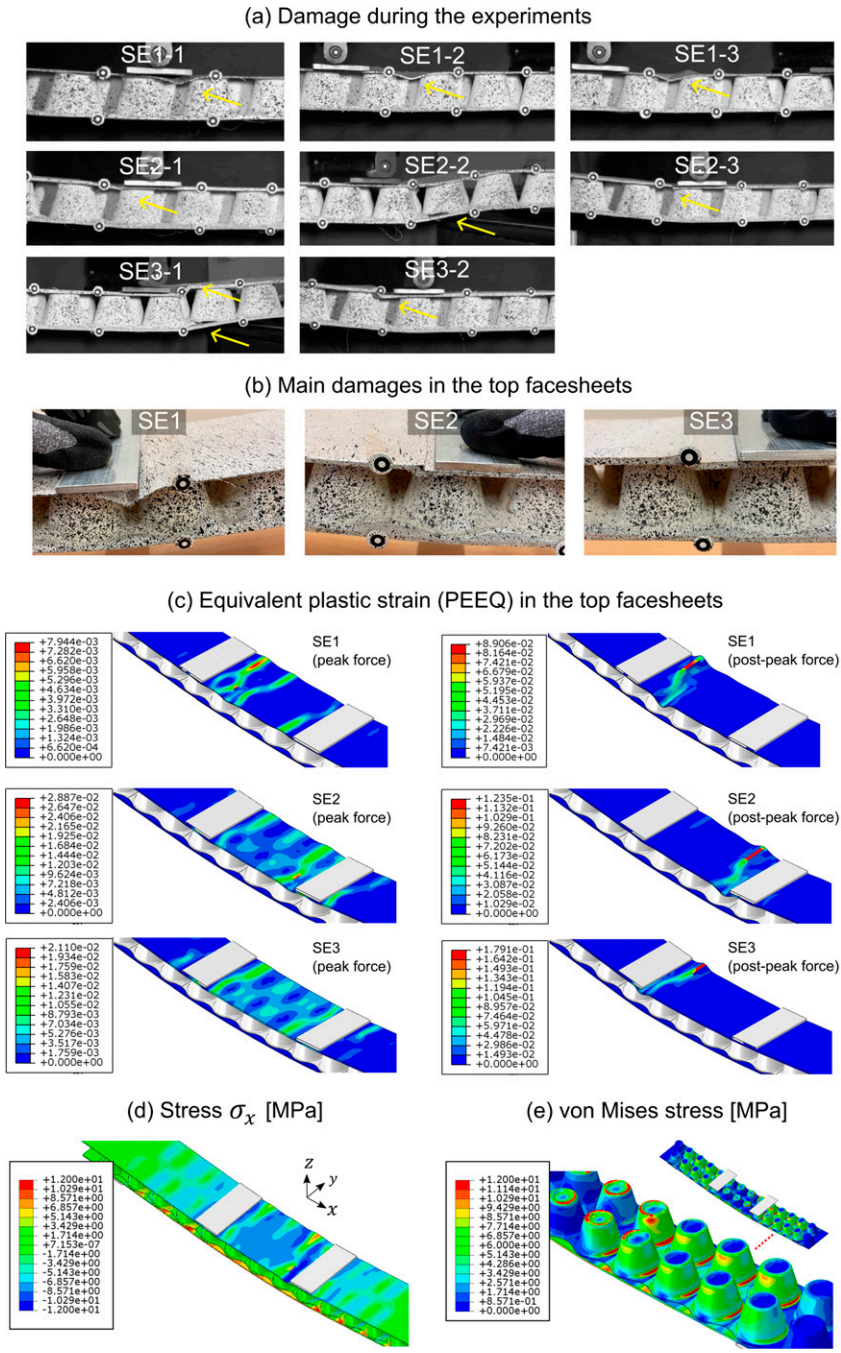

Figure 8. (a) Photo of the damage of each sample in the experiments, (b) typical damages that occurred in the top facesheets, (c) equivalent plastic strain at peak force and post-peak force (80% of the peak force) from the FE simulations, (d) stress in *x*-direction (σ_x) in SE2 at peak force and (e) von Mises stress in the core at peak force showing stress localization.

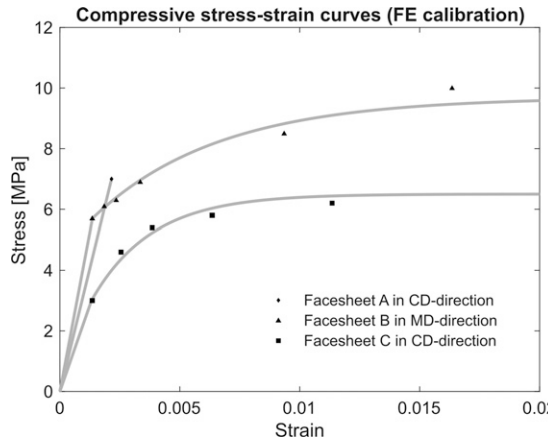

Figure 9. Stress-strain curves of the compression behaviour of the facesheets. The solid grey curves are fitted to the experimentally obtained values indicated by markers.

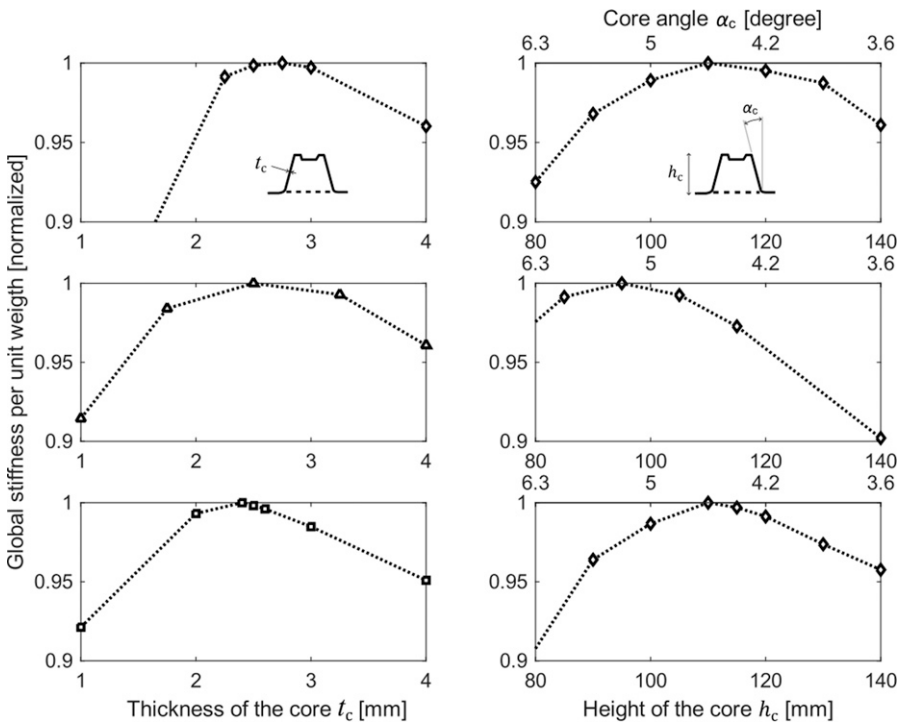

Figure 10. Global stiffness per unit weight for SE1, SE2 and SE3 beams: Graphs with optimum height of the core against core thickness on the left, and graphs with optimum thickness against the height of the core on the right.

stiffness with respect to the weight of the beam, $\Delta F/(\Delta w_{5,14}M)$, where M is total mass,[24] see Table 1. The total mass is directly calculated in Abaqus using *Mass properties* command.

From the paper processes, the shape of the core cups is more adjustable since it is manufactured by moulding, whereas the facesheets can only be adjusted by varying their thickness. For this study, we therefore considered the optimization for the core units only and assume the three facesheets A, B and C as references with their respective configurations SE1, SE2 and SE3. The parameters to be optimized are the thickness t_c, and height of the core h_c. The diameters of the lower parts of the cups in the core units are kept constant to not compromise neither the design of the cup-box core nor the beam width. A consequence of this choice is that the angle of the core α_c varies.

Figure 10 shows the normalized global stiffness per unit weight as a function of the parameters. The optimal values are obtained when the normalized global stiffness is 1. The figure is organized so that the thickness of the core t_c with optimized height h_c^{opt} is shown in the left-hand side of the three types of beams and the height of the core h_c, with optimized thickness t_c^{opt} on the right-hand side. The optimized values are $t_c^{opt} = 2.6$ mm and $h_c^{opt} = 110$ mm for SE1, $t_c^{opt} = 2.5$ mm and $h_c^{opt} = 95$ mm for SE2 and $t_c^{opt} = 2.4$ mm and $h_c^{opt} = 110$ mm for SE3, respectively. As a comparison to the stiffnesses of the beam obtained from the experimental tests, Figure 5(b) shows the stiffness with optimized cores (white markers) over the calibrated values from the section 3.1. For all three cases the optimum geometry considerably increases the flexural as well as the shear rigidity.

Conclusion

Innovative load-bearing sandwich beams with cup-box core produced in different configurations from paper materials were analysed in quasi-static bending. The top facesheets yielded first due to the lower strength in compression than in tension in paper materials. For this design, therefore, one of the critical design issues is the compressive strength of the top facesheets. The main initial failure was observed in the top facesheets, but there was a case of delamination of the core from the facesheet, which caused lower strength. Beams made of facesheets of thickness $t_f \approx 1$ mm were more susceptible to premature buckling failure, whereas those made of thicker facesheets ($t_f \geq 2$ mm) withstood buckling failure and behaved ductile due to yielding before failure. It was thus reaching higher beam deflections before failure.

The work has shown an alternative way to estimate elastic moduli of the facesheets along the beams via local bending stiffness using the displacements of DIC markers in the constant-moment regions. The flexural rigidity therefrom was estimated. Shear rigidities, which is strongly related to the in-plane elastic modulus of the core material, were estimated from the mid deflection and showed large scatter for all beam configurations. This scatter was mainly related to difficulties during the tests as the bending rigs allow rotations in all axis. That in turn occasionally caused twisting of the sandwich beams due to the asymmetry of the core, the

non-centered positions of the beams in the rigs and local non-intentional deformation at supports. The analysis of shear rigidities indicates that cup-box core outperformed some commercial foam cores. An attempt was made to compare the cup-box core to paper honeycomb cores, but the literature values vary due to differences in core shapes, core densities, material orientations and paper materials used and potentially climate conditions. This work suggests conducting similar analyses in the same experimental conditions for more accurate comparisons of sandwich element counterparts.

The developed FE model calibrated with the local bending stiffness and shear rigidities obtained good agreement with experiments in force-deflection diagrams including the prediction of peak load before the top-facesheet failure. It also predicted the development of plasticity and the diagonal buckling behavior in the compressed facesheets. For this analysis, the equivalent plastic strains are relevant to compare the FE results with the experimental observations. Once calibrated, the model is used to estimate the modulus of elasticity for the facesheet materials and the in-plane modulus of the core material. Furthermore, it is used to estimate the compressive initial yield stress and shapes of the hardening functions of the facesheets. In this aspect, this work suggests further investigations in conventional mechanical material tests for the studied paper materials to be compared to the material data obtained from the structural level tests performed herein.

Optimizing the global stiffness is an efficient way to design the cup-box core geometry using the developed FE model. For bending according to the presented load case, this study suggests that the optimal thickness and height of the core for all cases are in average t_c = 2.5 mm and h_c = 105 mm, which is approximately 3 times higher than the original values used.

Acknowledgements

Ecopals AB, Smurfit Kappa Sverige AB and Rottneros Packaging AB are acknowledged for supplying the materials and sharing their knowledge in pulp and paper processes. The authors are grateful for the research funding from the Knowledge Foundation (KKS), KK project number 20210063. Mr Maxim Nilsson and Mr Emil Lockner are also acknowledged for their assistance in the experimental tests.

Declaration of conflicting interests

The author(s) declared no potential conflicts of interest with respect to the research, authorship, and/or publication of this article.

Funding

The author(s) disclosed receipt of the following financial support for the research, authorship, and/or publication of this article: This work was supported by the Stiftelsen för Kunskaps-och Kompetensutveckling (20210063).

ORCID iD

Marcus Vinícius Tavares da Costa https://orcid.org/0000-0002-0491-1077

Supplemental Material

Supplemental material for this article is available online.

References

1. Söderholm P. The green economy transition: the challenges of technological change for sustainability. *Sustainable Earth* 2020; 3. DOI: 10.1186/s42055-020-00029-y.
2. United Nations. Transforming our world: The 2030 agenda for sustainable development. *United Nations*. 2015.
3. Didone M, Saxena P, Brilhuis Meijer E, et al. Moulded pulp manufacturing: overview and prospects for the process technology. *Packag Technol Sci* 2017; 30: 231–249. DOI: 10.1002/pts.2289.
4. Östlund S and Niskanen K. *Mechanics of paper products*. De Gruyter, 2021.
5. Mäkelä P and Östlund S. Orthotropic elastic–plastic material model for paper materials. *Int J Solid Struct* 2003; 40: 5599–5620. DOI: 10.1016/S0020-7683(03)00318-4.
6. Robertsson K, Engqvist J, Wallin M, et al. Out-of-plane uniaxial loading of paperboard: experimental procedure and evaluation. *Nord Pulp Pap Res J* 2023; 38: 389–398. DOI: 10.1515/npprj-2023-0017.
7. Stenberg N, Fellers C and Östlund S. Measuring the stress-strain properties of paperboard in the thickness direction. *J Pulp Pap Sci* 2001; 27: 213–221, article.
8. Joelsson T, Pettersson G, Norgren S, et al. High strength paper from high yield pulps by means of hot-pressing. *Nordic Pulp &. Paper Research Journal* 2020; 35: 195–204. DOI: 10.1515/npprj-2019-0087.
9. Alzweighi M, Mansour R, Tryding J, et al. Evaluation of Hoffman and Xia plasticity models against bi-axial tension experiments of planar fiber network materials. *Int J Solid Struct* 2022; 238: 111358. DOI: 10.1016/j.ijsolstr.2021.111358.
10. Li Y, Stapleton SE, Reese S, et al. Anisotropic elastic-plastic deformation of paper: in-plane model. *Int J Solid Struct* 2016; 100-101: 286–296. DOI: 10.1016/j.ijsolstr.2016.08.024.
11. Mäkelä P. On the fracture mechanics of paper. *Nord Pulp Pap Res J* 2002; 17: 254–274. DOI: 10.3183/npprj-2002-17-03-p254-274.
12. Wellmar P, Gregersen ØW and Fellers C. Prediction of crack growth initiation in paper structures using a J-integral criterion. *Nord Pulp Pap Res J* 2000; 15: 4–11. DOI: 10.3183/npprj-2000-15-01-p004-011.
13. Marin G, Nygårds M and Östlund S. Stiffness and strength properties of five paperboards and their moisture dependency. In: *Paper conference and trade show, PaperCon 2019, 5 may 2019 through 8 may 2019*. TAPPI Press, 2019, pp. 1193–1208.
14. Marin G, Nygårds M and Östlund S. Elastic-plastic model for the mechanical properties of paperboard as a function of moisture. *Nordic Pulp & Paper Research Journal*. 2020; 353–361. doi:10.1515/npprj-2019-0104.
15. Erkkilä A-L, Leppänen T, Puurtinen A, et al. Hygroexpansivity of anisotropic sheets. *Paper Research Journal* 2015; 30: 326–335. DOI: 10.3183/npprj-2015-30-02-p326-335.
16. Lif JO, Östlund S and Fellers C. Applicability of anisotropic viscoelasticity of paper at small deformations. *Mech Time-Dependent Mater* 1998; 2: 245–267. DOI: 10.1023/a:1009818022865.
17. Alfthan J. Micro-mechanically based modeling of mechano-sorptive creep in paper. In: *Doctoral thesis, comprehensive summary*. KTH, 2004.

18. Coffin DW. The creep response of paper. In: *Advances in paper science and technology*, 2018.
19. Robertsson K. *Continuum modeling of paperboard for the mechanical response of converting processes*. Lund University, 2023.
20. Marin G, Hagman A, Östlund S, et al. Torsional and compression loading of paperboard packages: experimental and FE analysis. *Packag Technol Sci* 2023; 36: 31–44. DOI: 10.1002/pts.2693.
21. Woodtube. Resource efficient products from the forest. https://wood-tube.com/ (2024).
22. Allen HG. *Analysis and design of structural sandwich panels*. Pergamon, 1969.
23. Ashby MF. *Metal foams a design guide*. Boston: Butterworth-Heinemann, 2000.
24. Gibson LJ and Ashby MF. *Cellular solids: structure and properties*. 2nd edn. Cambridge University Press, 1997.
25. Ren J, Zhou Y and Gao W. Bending response and failure characteristics of nomex honeycomb sandwich with continuous composite facesheet encasement. *J Sandw Struct Mater* 2023; 1: 10996362231172448. DOI: 10.1177/10996362231172448.
26. Zupan M, Chen C and Fleck NA. The plastic collapse and energy absorption capacity of egg-box panels. *Int J Mech Sci* 2003; 45: 851–871. DOI: 10.1016/S0020-7403(03)00136-X.
27. Ma Q, Rejab M, Siregar J, et al. A review of the recent trends on core structures and impact response of sandwich panels. *J Compos Mater* 2021; 55: 2513–2555. DOI: 10.1177/0021998321990734.
28. Kmita-Fudalej G, Szewczyk W and Kołakowski Z. Bending stiffness of honeycomb paperboard. *Materials* 2022; 16: 156. DOI: 10.3390/ma16010156.
29. Chen Z and Yan N. Investigation of elastic moduli of Kraft paper honeycomb core sandwich panels. *Compos B Eng* 2012; 43: 2107–2114. DOI: 10.1016/j.compositesb.2012.03.008.
30. Jivkov V, Simeonova R, Kamenov P, et al. Strength properties of new lightweight panels for furniture and interiors. In: *Proceedings of the 23rd International Scientific Conference "Wood Is Good–With Knowledge and Technology to a Competitive Forestry and Wood Technology Sector*. Zagreb, Croatia, 2012, pp. 49–58.
31. Fu Y and Sadeghian P. Bio-based sandwich beams made of paper honeycomb cores and flax FRP facings: flexural and shear characteristics. *Structures* 2023; 54: 446–460. DOI: 10.1016/j.istruc.2023.05.064.
32. Zenkert D. The handbook of sandwich construction. In: *Engineering Materials Advisory Services* 1997: 447.
33. Smardzewski J and Tokarczyk M. Lightweight honeycomb furniture panels with discreetly located strengthening blocks. *Compos Struct* 2024; 331: 117927. DOI: 10.1016/j.compstruct.2024.117927.
34. Pflug J, Vangrimde B, Verpoest I, et al. Continuously produced paper honeycomb sandwich panels for furniture applications. In: *5th Global Wood and Natural Fibre Composites Symposium Kassel*. Germany, 2004, pp. 27–28.
35. Isaksson P and Carlsson LA. Analysis of the out-of-plane compression and shear response of paper-based web-core sandwiches subject to large deformation. *Compos Struct* 2017; 159: 96–109. DOI: 10.1016/j.compstruct.2016.09.060.
36. Sting Bioeconomy. The innovative Greenwood from Ecopals is getting ready to enter the marketplace. https://stingbioeconomy.com/ (2023).
37. Christopher JB. *Handbook of pulping and papermaking*. San Diego: Academic Press, 1996.

38. EN 408:2010/A1:2012 Timber structures - structural timber and glued laminated timber - determination of some physical and mechanical properties.
39. Hill R. A theory of the yielding and plastic flow of anisotropic metals. *Proceedings of the Royal Society of London Series A Mathematical and Physical Sciences* 1948; 193: 281–297. DOI: 10.1098/rspa.1948.0045.
40. Dassault Systemes Simulia. *Abaqus analysis user's guide*. Dassault Systemes Corp, 2016.
41. Yeh K, Considine J and Suhling J. The influence of moisture content on the nonlinear constitutive behavior of cellulosic materials. In: Tappi Proceedings: 1991 International Paper Physics Conference, 1991.
42. Betts D, Sadeghian P and Fam A. Experimental behavior and design-oriented analysis of sandwich beams with bio-based composite facings and foam cores. *J Compos Construct* 2018; 22: 04018020.